Deciphering effects of chemical structure on azo dye decolorization/degradation characteristics: Bacterial vs. photocatalytic method

ARTICLE *in* JOURNAL OF THE TAIWAN INSTITUTE OF CHEMICAL ENGINEERS · SEPTEMBER 2012

Impact Factor: 3 · DOI: 10.1016/j.jtice.2012.03.001

Journal of the Taiwan Institute of Chemical Engineers 43 (2012) 760–766

Contents lists available at SciVerse ScienceDirect

Journal of the Taiwan Institute of Chemical Engineers

journal homepage: www.elsevier.com/locate/jtice

Deciphering effects of chemical structure on azo dye decolorization/degradation characteristics: Bacterial vs. photocatalytic method

Qian Zhang [a], You Hai Jing [a], Angus Shiue [b], Chang-Tang Chang [c,d,*], Bor-Yann Chen [d,e,**], Chung-Chuan Hsueh [e,***]

[a] College of Oceanography and Environmental Science, Xiamen University, China
[b] Graduate Institute of Mechanical and Electrical Engineering, National Taipei University of Technology, Taiwan
[c] Department of Environmental Engineering, National I-Lan University, Taiwan
[d] Center of Green Technology (G-TEC), National I-Lan University, Taiwan
[e] Department of Chemical and Materials Engineering, National I-Lan University, I-Lan 260, Taiwan

ARTICLE INFO

Article history:
Received 13 July 2011
Received in revised form 23 November 2011
Accepted 1 March 2012
Available online 28 April 2012

Keywords:
Bacterial decolorization
Photodegradation
Azo dye
Chemical structure

ABSTRACT

This study tended to kinetically disclose comparative assessment on characteristics of azo dye decolorization/degradation via bacterial and abiotic treatment. The result revealed that the ranking of abiotic degradation performance via photocatalysis was RB5 > RR198 > DY86 > RR141 > RB171 ≈ RG19 > RY84. In contrast, the ranking of bacterial decolorization was RR198 > RB5> RR141 > DY86 > RB171 > RY84 > RG19. Photocatalytic degradation of azo dyes was conducted by complete oxidation; however, dye biodegradation was carried out through reductive decolorization. For photodegradation, azo dyes containing electron-releasing groups (*e.g.*, amino group in RB5) around azo bond would be more vulnerable for color removal than those with the electron-withdrawing groups (*e.g.*, sulfo group in RB171, RG19 and RR141). On the other hand, azo dyes containing more electron-withdrawing groups (*e.g.*, RR198, RB5 and RR141) in the proximity of azo bond(s) would be biodegraded in faster rates. This study disclosed that both the rate of photodegradation and biodegradation were significantly affected by the steric hindrance and electron density near the azo bond. Evidently, photodegradation would proceed in higher rates than biodegradation. In addition, complete mineralization of photodegradation could prevent the accumulation of intermediates via reductive biodegradation for clean-up of dye pollutants.

1. Introduction

As known, dyestuff and dyeing industry have long been the important traditional industries in the world. It was estimated that *ca.* 0.7 million tons of dye were used per year, including 50% of azo dyes [1]. Environmental sectors also evaluated that *ca.* 15% of the synthetic textile dyes used in industry were still released in waste streams during manufacturing or processing operations [2]. Inevitably, the treatment of dye-containing wastewater was one of top-priority issues to environmental protection, as dye-containing wastewater is in high COD (chemical oxygen demand), low biodegradability (*i.e.*, $BOD_5/COD < 0.2–0.3$ [1,3]). To achieve complete degradation of dye-bearing wastewater, inevitably an economically-feasible means of degradation was needed for cradle-to-cradle design to sustainable development. In fact, advanced oxidation processes (AOPs) are the most frequently selected alternatives and hence attracted attentions recently [4–6].

Although the mechanism(s) of photodegradation have been proposed in literature, all reports were solely mentioned for the possible routes of dye degradation (*e.g.*, intermediates identified for pathway of dye degradation). All studies were consistent to show that azo-bond structure seemed to be the most vulnerable in degradation of azo dye. For example, Bauer et al. [2] and Vinodgopal et al. [7] all showed that the degradation of azo dyes was triggered in the proximity of azo bond (*i.e.*, –N=N–). Their studies showed that the azo dye molecule was cleaved at the chemical bonding(s) next to azo bond that is attached to the naphthalene moiety (*e.g.*, Φ_1–N=N–$\Phi_2 \rightarrow \Phi_1 = O + \Phi_2 + N_2 + NO_3^-$ for oxidative degradation). Feng et al. [8] showed that the hydrogenated azo structure was destroyed, resulting in the generation of benzene and naphthalene via photodegradtioncatalytic reaction. Plus, Zhou and He [9] explored

* Corresponding author. Tel.: +886 3 931 7580.
** Corresponding author at: Department of Chemcial and Materials Engineering, NIU, I-Lan 260, Taiwan. Tel.: +886 3 931 7497; fax: +886 3 9357025.
*** Corresponding author. Tel.: +886 3 931 7502; fax: +886 3 9357025.
E-mail addresses: ctchang@niu.edu.tw (C.-T. Chang), boryannchen@yahoo.com.tw, bychen@niu.edu.tw (B.-Y. Chen), cchsueh@niu.edu.tw, cchsueh88@gmail.com (C.-C. Hsueh).

1876-1070/$ – see front matter © 2012 Taiwan Institute of Chemical Engineers. Published by Elsevier B.V. All rights reserved.
doi:10.1016/j.jtice.2012.03.001

three advanced oxidation processes (*i.e.*, wet oxidation, electrochemical oxidation and wet electrochemical oxidation) to degrade azo dye(s), and all of first step for dye destruction was to break azo structure.

As mentioned previously, literature usually proposed possible pathways for reaction mechanisms of dye degradation via identification of the derived intermediates. Here, this first-attempt study tended to clarify how the chemical structure (*e.g.*, electron-donating or electron-withdrawing group(s)) affected the degradability of azo dye(s). According to degradation data for seven model azo dyes, the findings showed that photocatalytic degradation and bacterial decolorization of azo dyes were carried out via oxidative degradation and reductive decolorization, respectively. Apparently, the presence of electron-withdrawing or donating groups near azo bond(s) significantly affected dye degradability/decolorization. In addition, both abiotic and biotic degradation of azo dye(s) were significantly affected by the steric hindrance and electron-density profiles around azo bond(s). This finding could systematically provide a guideline to identify characteristics of degradability and recalcitrance of azo dye(s) for environmental protection via abiotic and biotic treatment.

2. Materials and methods

2.1. Chemicals

Seven azo dyes (Reactive Black 5 (RB5), Reactive Blue 171 (RB171), Reactive Green 19 (RG19), Reactive Red 198 (RR198), Reactive Red 141 (RR141), Direct Yellow 86 (DY86), Reactive Yellow 84 (RY84); all purchased from Everlight Chemical Ltd., Taipei, Taiwan) were selected for study (Fig. 1). The commercial TiO_2 catalyst P25 was purchased from ACROS.

2.2. Analytical methods

The concentration of dyes (RB5 (λ_{max} = 600 nm), RB171 (λ_{max} = 609 nm), RG19 (λ_{max} = 631 nm), RR198 (λ_{max} = 522 nm), RR141 (λ_{max} = 544 nm), DY86 (λ_{max} = 393 nm), RY84 (λ_{max} = 411 nm)) was detected by UV–vis spectrophotometer (Hitachi, U-3900) with appropriate calibrations at specific wavelengths (λ_{max}). The photocatalytic degradation column reactor used in this study was an annular quartz glass tube, which height is 0.45 m and the diameter of the bottom is 0.05 m. The photocatalytic degradation of dyes in the presence of UV light (14 W) with a maximum wavelength of 254 nm, and using self-producted Pt–TNT as photocatalysts (at the dosage of 4 g/L). During reaction cooling water was circulated around the sample container continuously to maintain the reaction solution isothermally at 25 °C. The pHs of test solutions of azo dyes were not adjusted (*ca.* 6.7–7.1), as the zero-charge point of TiO_2 (P25) was *ca.* at pH 6.8 [10]. In fact, pH level of azo dye solution has significant effects on photocatalytic reaction to be taking place; thus, pHs were not altered for experiments. Moreover, these unadjusted pHs for dye experiments were to simulate practical situation for green wastewater treatment. A TOC detector (Dohrmann, Phoenix 8000) was used to detect the organic concentration for calculating mineralization efficiency.

2.3. Preparation of TNT

Commercial TiO_2 (P25) nanoparticles (5.0 g) were mixed in 10.0 M $NaOH_{(aq)}$ solution and charged into a Teflon-lined autoclave. The autoclave was then oven-heated at 135 °C for 3 days. The precipitate was filtered and washed to obtain the resultant products. Then, test samples were finally obtained by calcination under the temperatures of 400 °C.

2.4. Preparation of Pt–TNT by photodeposition

An appropriate amount of TNT suspension solution was prepared in a Pyrex glass container. Then, the mixed solution was purged with nitrogen for 2 h to remove residual dissolved oxygen (DO) from of the solution. Then, an appropriate amount of H_2PtCl_6 $6H_2O$ was well mixed with 10 mL methanol to be formed as a test TNT solution. Photodeposition was performed for 8 h under a continuous nitrogen purge using a 254 nm ultraviolet light. Once the Pt–TNT suspension solution was formed, the subsequent clearing was applied through methods similar to those used with the TNT photocatalyst. The crystalline structures of TNT and Pt–TNT were characterized by X-ray diffraction (XRD) with Cu Ka radiation using an automated X-ray diffractometer (Shimazu Labx XRD-6000).

3. Results and discussion

3.1. Characterization of TNT and Pt–TNT

The XRD patterns of TNT and Pt/TNT are presented in Fig. 2. In XRD patterns of TNT and Pt/TNT, the peaks at 25.4, 37.8, 48.1 and 55.1° are assigned to the (1 0 1), (0 0 4), (2 0 0), (2 1 1) lattice planes, which are attributed to the signals of the anatase phase. The formation of the catalytically inactive rutile phase starts, as shown by the appearance of its (1 0 1) reflection at ~25.4°. All the peaks can be perfectly indexed as the body-centered tetragonal lattice structure [JCPDS no. 89-4921] of TiO_2, with lattice constants a = 3.772 Å, b = 3.772 Å and c = 9.52 Å. There is large difference in two curves; thus, doping platinum is highly monodispersed in the TNT.

3.2. Decolorization of azo dyes

As shown in Fig. 3 for time courses of dye degradation (or decolorization), the ranking of degradation (or decolorization) rate of seven dyes at the initial two hours, in decreasing order, was RB5 > RR198 ~ RR141 > DY86 ~ RG19~RB171 > RY84. According to Julson and Ollis [11], the degradation of azo dyes could be summarized to two steps just as shown below:

$$\text{Dye} \xrightarrow{k_1} \text{Intermediate(s)} \xrightarrow{k_2} \text{colorless product(s)}$$

where k_1 and k_2 is the first order rate constants of the two serial steps of proposed mechanism, respectively. As the proposed kinetics revealed, one could obtain analytical solution for time-series profiles of dye degradation as follows:

$$\text{Abs}_t = \text{Abs}_0\left(\left(k_3\frac{k_1}{k_2-k_1}\right)(e^{-k_1t}-e^{-k_2t})+e^{-k_1t}\right) \quad (1)$$

where Abs_t was the adsorption density at time t, Abs_0 denoted the absorption density of original sample. The kinetic constant k_3 is the constant related to the ratio of adsorption of dye and intermediate. The constants of k_1, k_2 and k_3 can be calculated through the equations as shown below:

$$\frac{\text{Abs}_t}{\text{Abs}_0} = (k_3-1)k_1t+1 \quad (2)$$

$$\ln\left(\frac{\text{Abs}_t}{\text{Abs}_0}\right) = -k_2t+\ln\left(-\frac{k_3k_1}{k_2-k_1}\right) \quad (3)$$

The data obtained from Eq. (1) all showed the best fitted to experimental data (Fig. 4). As explained above, the rate constant of k_1 showed the degradation of dyes and thus was chosen to be the indicator kinetic variable for degradation of dyes.

A

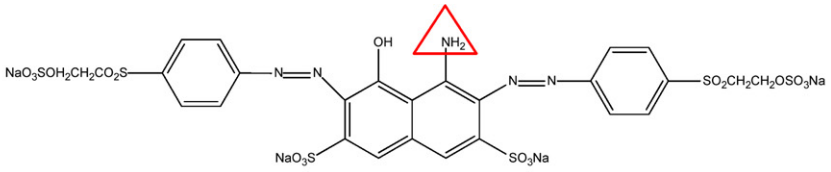

Reactive Black 5 (RB5)

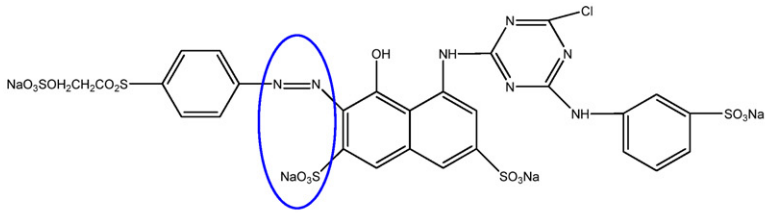

Reactive Red 198 (RR198)

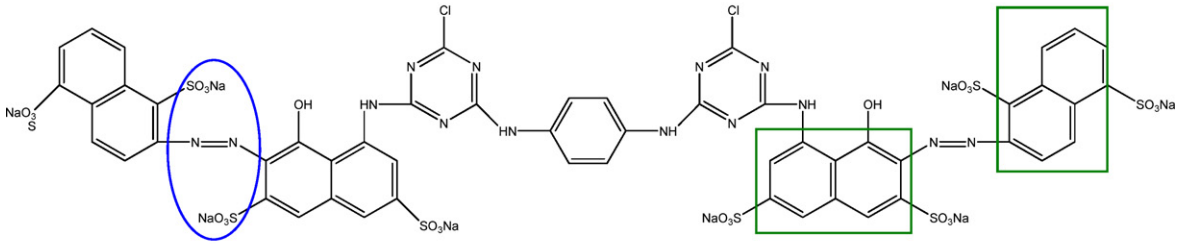

Reactive Red 141 (RR141)

B

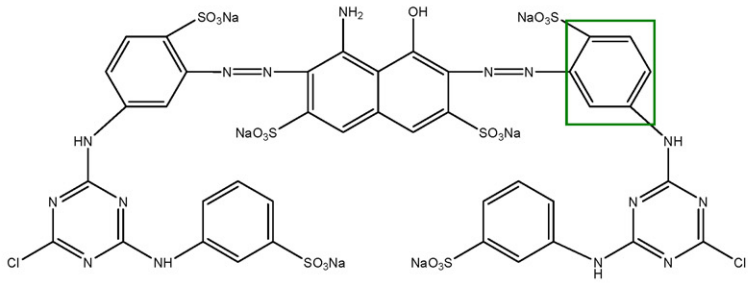

Reactive Blue 171 (RB171)

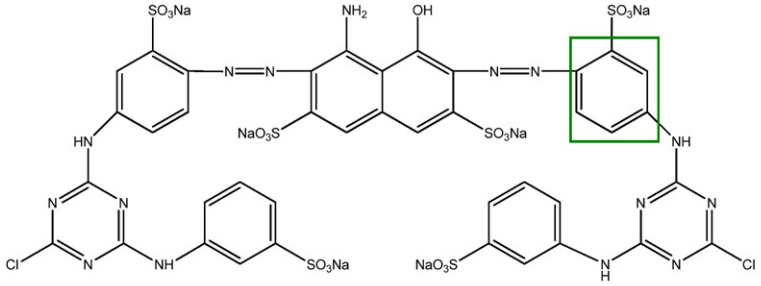

Reactive Green 19 (RG19)

Fig. 1. The structures of the seven dyes (A) Reactive Black 5 (RB5), Reactive Red 198 (RR198), and Reactive Red 141 (RR141), (B) isomeric dyes – Reactive Blue 171 (RB171), and Reactive Green 19 (RG19), (C) non-naphthol type azo dyes – Direct Yellow 86 (DY86), and Reactive Yellow 84 (RY84). The red triangle is the main difference that affects the degradation rate of RB5 from RR198. The blue rings show the difference between RR198 and RR141. The green rectangles show the reason of RR141 $>$ RB171 $\sim$ RG19. The purple trapezoids are the main reasons of degradation rate for DY86 $>$ RY84. (The details could be seen in Section 3.2). (For interpretation of the references to color in this figure legend, the reader is referred to the web version of the article.)

C

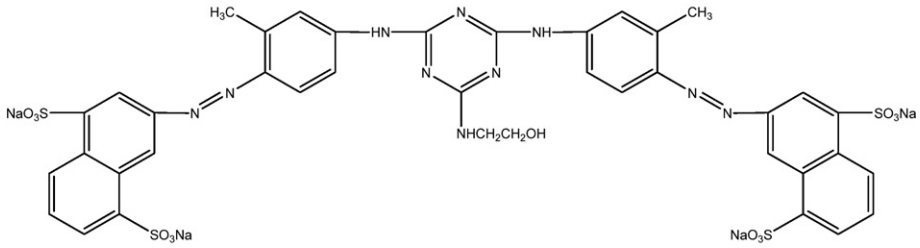

Direct Yellow 86 (DY86)

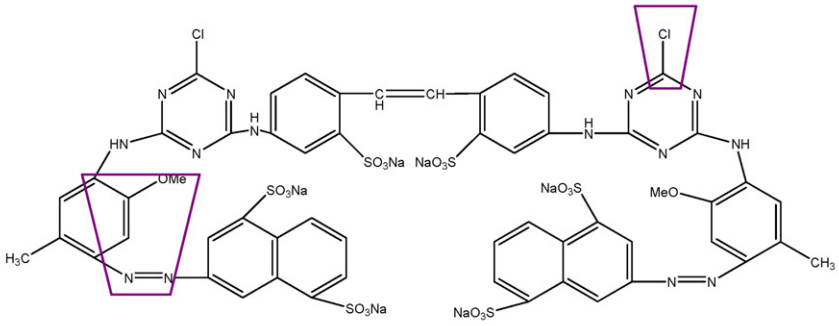

Reactive Yellow 84 (RY84)

Fig. 1. (*Continued*).

The ranking of degradation rate constant (1/(h μM)) through photocatalytic oxidation was RB5 (1.590) > RR198 (0.440) > DY86 (0.415) > RR141 (0.305) > RB171 (0.296) ~ RG19 (0.295) > RY84 (0.165).

The rate of oxidation and reduction for azo dyes is strongly related to the nucleophilicity and electrophilicity of azo dyes, respectively [12,13]. That is, molecules in excellent nucleophilicity simply indicated molecules in a great electron-releasing capability to be oxidized. On the other side, molecules in electrophilicity implied that these molecules were in electron-deficiency to be reduced. When azo dyes contained various subsituents in the proximity of azo bond(s), these subsituents could thus be divided into electron-releasing groups (ERGs) (*e.g.*, amino group, H_2N– or hydroxyl, HO– or alkyl group, R–) and electron-withdrawing groups (EWGs) (*e.g.*, sulfo group, $–SO_3^-$, sulfonyl group, $–SO_2(CH_2)_nSO_4^-$, or halo group, F, Cl [12,14]). These subsituents would influence the electron density near azo bond(s) to affect decolorization rates of these azo dyes. For example, azo dyes containing ERGs around azo bond(s) would increase the nucleophilicity of azo dye(s) [12,15,16]. Plus, when an azo dye was oxidatively degraded, it would lose an electron to be a positively charged intermediate as shown in intermediates b–i of Fig. 5 [2,7,17]. Azo dyes containing ERGs (*e.g.*, subsituent Y as ERGs of intermediates b–i in Fig. 5) could be stably oxidized to be positively-charged via inductive or resonance effect [14], providing favorable conditions for oxidative decolorization. On the other side, azo dyes containing EWGs would significantly suppress the oxidation of azo dye [15,16].

Here, this study found that both rate of photodegradation and bacterial decolorization were considerably affected by the steric hindrance and electron density around the azo bond [18]. The reasoning to cause such phenomena was straightforward as follows:

(1) Azo dyes containing stronger ERGs, fewer EWGs, and less steric hindrance (*e.g.*, RB5) would be more easily to be oxidized. Among seven test azo dyes, RB5 apparently showed the fastest rate for oxidative degradation via TiO_2 photocayalysis. Due to relatively strong electron-releasing characteristics of amino and hydroxyl (H_2N– and HO–) groups at *ortho* to azo bond (–N=N–) in RB5 (Fig. 1), both ERGs would increase the electron density around azo bond. Plus, the amino group has a greater electron-releasing capability than hydroxyl group [14]. In addition, RB5 could be further oxidized to be a more stable positively-charged intermediate due to the presence of both ERGs via inductive and/or resonance effect (*e.g.*, subsituent Y as ERGs of intermediates b-i shown in Fig. 5). Thus, azo dyes with ERGs were more easily to be oxidized due to higher electron densities near azo bond(s) [12,15,16]. Moreover, RB5 had fewer EWGs (*i.e.*, one sulfo group at *ortho* to azo bond) compared to other test azo dyes (*e.g.*, two sulfo groups at *ortho* to azo bond of RR141, RB171 or RG19; Fig. 1). In addition, RB5 had less steric hindrance around azo bond, these all provided kinetically more favorable conditions for oxidative decolorization than other test azo dyes. Regarding second rank-RR198, it also owned substituent characteristic similar to RB5 (Fig. 1); however, RR198 owned only one hydroxyl group at *ortho* to azo bond (*i.e.*, absence of an amino group compared to RB5) with the lower electron density around azo bond compared to RB5. In contrast, for reductive decolorization this lower electron-density of RR198 resulted in its higher rate of bacterial decolorization than RB5 [18]. Thus, more electrophilicities of azo dyes with lower electron density were more favorable for reductive biodecolorization of azo dyes [13,18].

(2) Azo dyes with more EWGs (*e.g.*, sulfo group, $–SO_3^-$) and/or more steric hindrance around azo bond would be more resistant to oxidative decolorization (*e.g.*, isomers RB171 and RG19 (Fig. 1) with approx. identical rate constant). Although

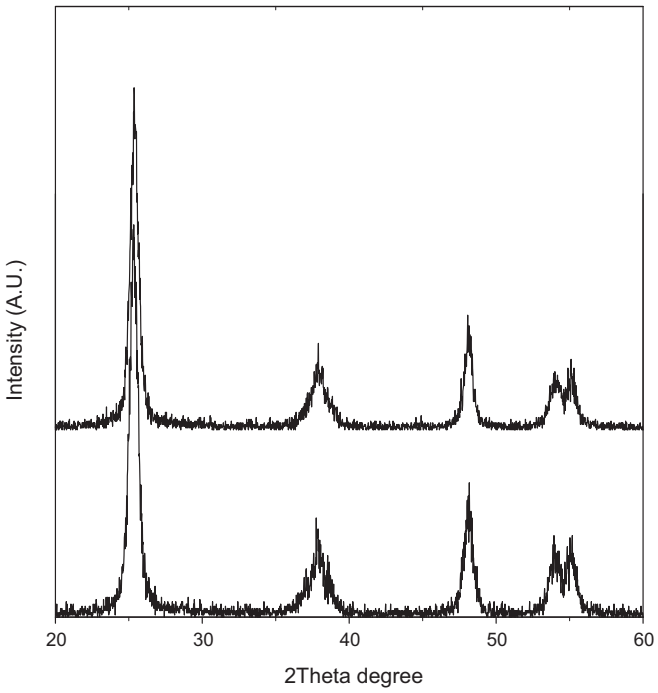

Fig. 2. The XRD patterns of the TNT (a) and Pt–TNT (b) (from up to down).

RB5, RB171 and RG19 are all synthesized from H acid (*i.e.*,

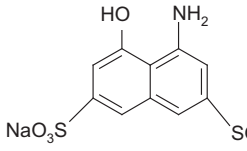

) to produce diazo dyes, RB5 has only one EWG (sulfo group) at *ortho* to azo bond. However, RB171and RG19 with two sulfo groups at *ortho* to azo bond not only decreased the electron density around azo bond via inductive and resonance effect (*i.e.*, intermediates b–i in Fig. 5), but also increased the steric hindrance. Both factors provoked more resistance to oxidation of isomers RB171 and RG19. Plus, similar steric-hindrance phenomenon might be seen for RR141 (more steric-hindrance) vs. RR198 (less steric-hindrance). The decolorization rate constant of RR141 (0.305/(h μM)) was lower than that of RR198 (0.440/(h μM)) due to more sulfo groups present around azo bond in RR141. As a matter of fact, the steric hindrance also significantly interferes with oxidative degradation of azo dyes via abiotic TiO_2 photocatalysis. For example, Direct Fast Scarlet 4BS was easier to be oxidized than Acid Red 3B, since Acid Red 3B contained more substituents aroud azo bond [19]. Plus, the color removal efficiency of methyl orange and Chicago sky blue 6B were 98.5% and 60.3%, respectively, since Chicago sky blue 6B contained more substituents aroud azo bond [20]. In fact, a similar example of such steric hindrance effect could also be seen on reductive biodecolorization for RR198, RB5 > RR141 [18].

(3) Regarding non-naphthol type azo dyes DY86 and RY84 (Block C in Fig. 1), they are very different from the other five dyes due to the absence of hydroxyl groups at *ortho* to azo bond (Fig. 1). Due to only one weak ERG (*e.g.* methyl) at *ortho* to azo bond and lack of strong ERGs (*e.g.* $-NH_2$ or –OH) in RY84, the oxidative degradation rate of RY84 was ranked the slowest degradation of seven test azo dyes. In addition, one methoxy group (CH_3O-) could

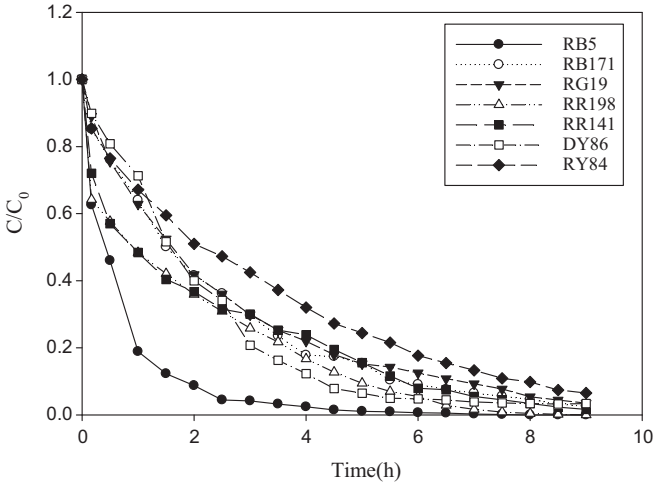

Fig. 3. Time courses of photocatalytic degradation of seven azo dyes.

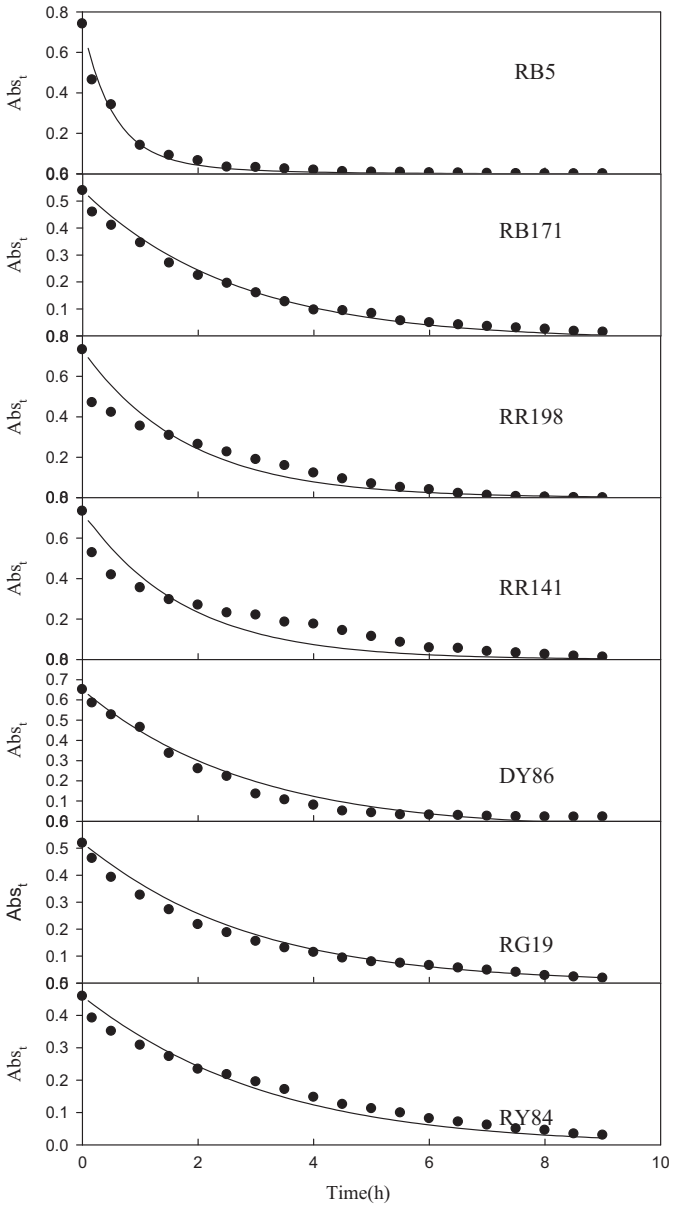

Fig. 4. Comparison of predicted and experimental time-series profiles of dye degradation via TiO_2 photodegradation.

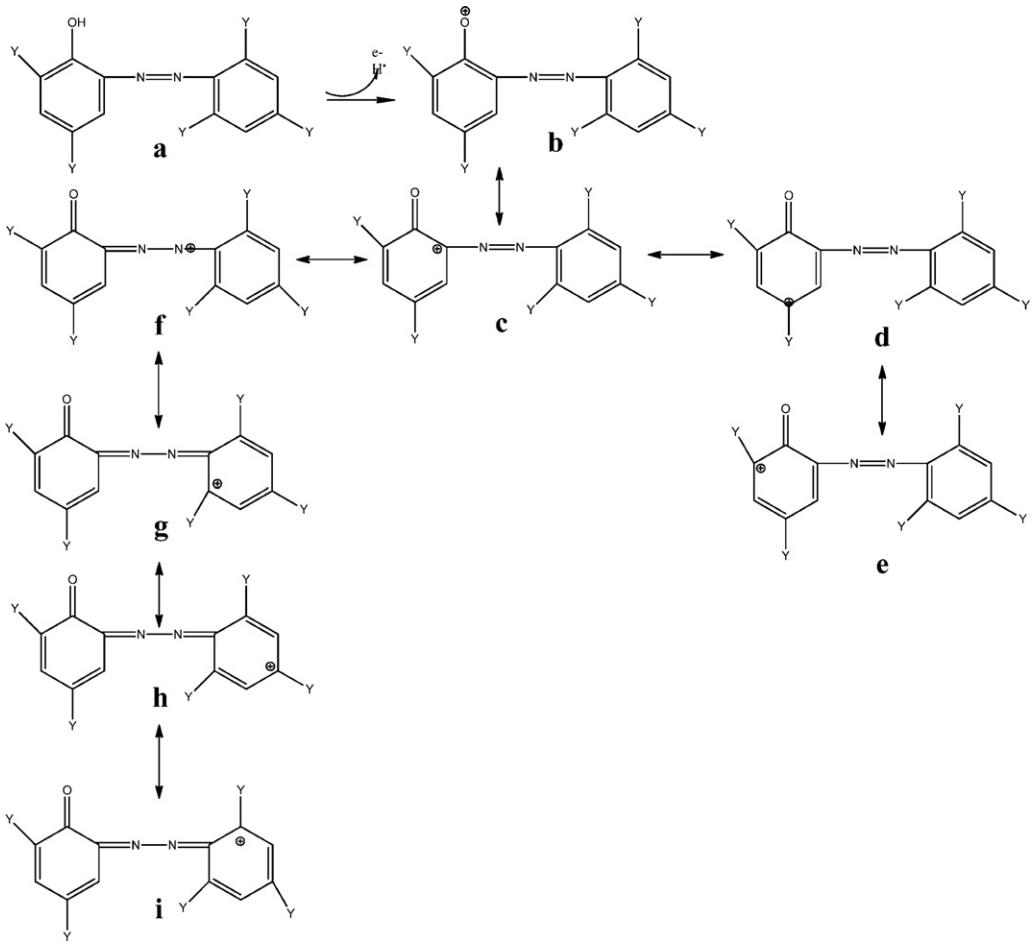

Fig. 5. The resonance forms of cationic intermediate in oxidative degradation for azo dyes. As Y were the electron-releasing groups (ERGs) (*e.g.*, amino group, H_2N– or hydroxyl, HO– or alkyl group, R–), Y would be stably oxidized to be positively-charged via inductive or resonance effect, providing favorable conditions for oxidative decolorization.

exhibit as an EWG via inductive effect when it was at *meta* to azo bond in RY84 as shown below:

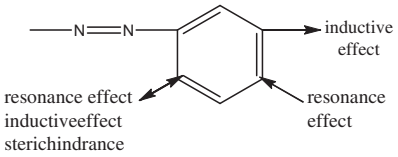

(note that methoxy group might be an ERG at *para* and *ortho* to azo bond by resonance effect [12]). In addition, one chloro atom with high electronegativity (as an EWG) bonded to1,3,5-triazine in RY84 (Block C in Fig. 1). All these conditions would result in significant decreases in electron density near azo bond of RY84 and thus RY84 ranked last for oxidative degradation of dyes. However, as one ERG (–$NHCH_2CH_2OH$) bonded to 1,3,5-triazine in DY86, this caused DY86 with more electron density to be faster oxidative decolorization than RY84. Regarding one methyl group at *ortho* to azo bond in DY86, methyl group is a less activating group as ERG than hydroxyl group in RR198 [14] and thus a lower electron density of DY86 than RR198 was expected. Therefore, the rate constant of DY86 was lower than that of RR198.

The oxidation rate constant of DY86 > RR141 could be explained as follows: the EWG (*e.g.*, sulfo group) at *ortho* and/or *para* to azo bond in RR141 would more significantly decrease the electron density of azo bond via inductive and/or resonance effects than the EWG (*e.g.*, sulfo group) at *meta* to azo bond in DY86 [14,18]. In addition, EWG (*e.g.*, sulfo group) at *ortho* and/or *para* to azo bond in RR141 would destabilize the cationic intermediate(s) of the oxidation via inductive and/or resonance effects (*e.g.*, intermediates b–i in Fig. 5). Thus, a slower rate of RR141 than DY86 was resulted. However, for reductive decolorization apparently RR141 would be faster than DY86 since RR141 was in a lower electron-density around azo bond for more electrophilicity [18].

(4) Azo dyes with polycyclic aromatic hydrocarbons (or PAHs) will be easier to be reduced and oxidized than those with benzenes (Φs) [21]. This was due to that the energy gap between HOMO (highest occupied molecular orbital) and LUMO (lowest unoccupied molecular orbital) would become lessening with more conjugative π bonds to be more easily decolorized [12]. In fact, this effect of low energy gap was seen in both reductive and oxidative decolorization. For instance, RR141 (*i.e.*, two naphthalenes around azo bonds) was faster to be oxidatively degraded than RB171 and RG19 (*i.e.*, only one H acid around azo bond in Fig. 1). This finding might also be seen in Hsueh et al. (*i.e.*, RR141 > RB171) [18]. Similar phenomenon was also observed by Gonçalves et al. [21] "... dyes of the β-naphthol type 2 and 4 lose colour faster than dyes derived from N,N-dimethylaniline."

3.3. Abiotic vs. biotic decolorization

3.3.1. Abiotic oxidative photodegradation vs. bio-oxidactive decolorization

Regardless of abiotic oxidative photodegradation or bio-oxidactive decolorization, more ERGs around azo bond(s) would

increase the rate of oxidative decolorizaiton due to increases of electron density of azo bond(s). On the contrary, EWGs at azo dyes would decrease the rate of oxidative decolorizaiton [15,16]. Since oxidants are electron-deficient, the electrophilic oxidants favor to react with azo bond(s) with high electron densities. In addition, azo dyes would lose electron(s) to be a positively charged intermediate(s) during oxidative degradation. Plus, azo dyes containing ERGs (*e.g.*, Y as ERGs in intermediates b–i of Fig. 5) would be stably oxidized to be positively-charged intermediate(s) via inductive or resonance effect. This provided favorable conditions for oxidative decolorization.

3.3.2. Abiotic oxidative photodegradation vs. bioreductive decolorization

Comparing the rankings of the results of abiotic oxidative photodegradation and bioreductive decolorization were slightly different, since different charged intermediate(s) were formed in two decolorization methods for azo dyes [2,7,17,18]. The ranking of oxidative degradation rate constant ($1/(\mu M\ h)$) by photocatalysis was RB5 > RR198 > DY86 > RR141 > RB171 ≈ RG19 > RY84 (*i.e.*, this study). In contrast, the ranking of bacterial reductive decolorization rate ($\mu M/ODU\ h^{-1}$), recalculated from Hsueh et al. [18] was RR198 (264.2) > RB5 (81.6) > RR141 (37.5) > DY86 (29.0) > RB171 (25.4) > RY84 (20.7) > RG19 (16.4). RB5 and RR198 had the fastest rate of decolorization among azo dyes in both decolorization methods, due to both azo dyes with less steric hindrance around azo bonds (Fig. 1). For photodegradation, azo dyes containing ERGs (*e.g.*, amino group in RB5) around azo bond would be easier for color remove than those with the EWGs (*e.g.*, sulfo group in RB171, RG19 and RR141). The more electron density around azo bond of RB5 was more easily to be oxidized than RR198; however, RB5 was less favorable for reductive biodecolorization. Azo dyes with sulfo groups at *para* and/or *ortho* to azo bond(s) showed more significant resonance effects to withdraw electrons from azo bond than those at *meta*, causing azo dyes to be in higher electrophilicities for faster reductive biodecolorization (*e.g.*, RR141 > DY86). However, the result would be reversed by oxidative photodegradation. Photo-oxidative degradation and bioreductive degradation were different in reaction mechanisms due to its different charged intermediates to result in their diverse nucleophilicity and electrophilicity. In summary, both degradations for decolorization were still strongly affected by the steric hindrance, electron density around the azo bond and energy gap between HOMO and LUMO of azo dyes. For both decolorization, apparently complete mineralization of photodegradation could prevent the accumulation of intermediates via reductive biodegradation for clean-up of dye pollutants.

4. Conclusion

The findings showed that both biotic and abiotic degradation affected by the steric hindrance and electron density around azo bond(s). For oxidative photodegradation, the presence of ERGs around azo bond(s) could increase the rate of reaction. In contrast, the existence of EWGs would repress rate of dye degradation. However, too many substituents around azo bond would increase the effect of steric hindrance to obstruct the decolorization reaction.

Acknowledgments

The authors sincerely appreciate financial support (NSC 99-2221-E-197-011-MY3 and NSC 99-2221-E-197-014) from Taiwan's National Science Council and from Taiwan's Ministry of Ecomic Affairs (MOEA 99-EC-17-A-10-S1-151) for this research.

References

[1] Zhao W, Wu Z, Shi H, Wang D. UV photodegradation of azo dye diacryl red X-GRL. J Photochem Photobiol A 2005;171:97.
[2] Bauer C, Jacques P, Kalt A. Photooxidation of an azo dye induced by visible light incident on the surface of TiO_2. J Photochem Photobiol A 2001;140:87.
[3] Hu C, Yu JC, Hao Z, Wong PK. Photocatalytic degradation of triazine-containing azo dyes in aqueous TiO_2 suspensions. Appl Catal B Environ 2003;42:47.
[4] Guo J, Du Y, Lan Y, Mao J. Photodegradation mechanism and kinetics of methyl orange catalyzed by Fe(III) and citric acid. J Hazard Mater 2011;186:2083.
[5] Rauf MA, Meetani MA, Hisaindee S. An overview on the photocatalytic degradation of azo dyes in the presence of TiO_2 doped with selective transition metals. Desalination 2011;276:13.
[6] Bansal P, Sud D. Photodegradation of commercial dye, procion blue HERD from real textile wastewater using nanocatalysts. Desalination 2011;267:244.
[7] Vinodgopal K, Wynkoop DE, Kamat PV. Environmental photochemistry on semiconductor surfaces: photosensitized degradation of a textile azo dye acid orange 7, on TiO_2 particles using visible light. Environ Sci Technol 1996;30:1660.
[8] Feng W, Nansheng D, Helin H. Degradation mechanism of azo dye C I. Reactive red 2 by iron powder reduction and photooxidation in aqueous solutions. Chemosphere 2000;41:1233.
[9] Zhou M, He J. Degradation of azo dye by three clean advanced oxidation processes: wet oxidation, electrochemical oxidation and wet electrochemical oxidation – a comparative study. Electrochim Acta 2007;53:1902.
[10] Konstantinou IK, Albanis TA. TiO_2-assisted photocatalytic degradation of azo dyes in aqueous solution: kinetic and mechanistic investigations – a review. Appl Catal B Environ 2004;49:1.
[11] Julson AJ, Ollis DF. Photocatalytic degradation of organic dyes by titanium dioxide in an air-catalyst system. M.S. thesis. USA: The Graduate Faculty of North Carolina State University; 2005 [also seen in the Proceedings for Photocatalytic And Advanced Oxidation Processes for Treatment of Air, Water, Soil, And Surfaces, 2005].
[12] Carey FA, Sundberg RJ. Structure and mechanisms. In: Advanced organic chemistry part A5th ed., Springer: USA; 2008. p. 411, 299, 989.
[13] Knackmuss HJ. Basic knowledge and perspectives of bioelimination of xenobiotic compounds. J Biotechnol 1996;51:287.
[14] McMurry J. Chemistry of benzene: electrophilic aromatic substitution. In: Organic chemistry6th ed., California: Brooks/Cole, Belmont; 2004. p. 541 [chapter 16].
[15] Suzuki T, Timofei S, Kurunczi L, Dietze U, Schüürmann G. Correlation of aerobic biodegradability of sulfonated azo dyes with the chemical structure. Chemosphere 2001;45:1.
[16] Pasti-Grigsby MB, Paszczynski A, Goszczynski S, Crawford DL, Crawford RL. Influence of aromatic substitution patterns on azo dye degradability by *Streptomyces* spp. and *Phanerochaete chrysosporium*. Appl Environ Microbiol 1992;58:3605.
[17] Stolz A. Basic and applied aspects in the microbial degradation of azo dyes. Appl Microbiol Biotechnol 2001;56:69.
[18] Hsueh CC, Chen BY, Yen CY. Understanding effects of chemical structure on azo dye decolorization characteristics by *Aeromonas Hydrophila*. J Hazard Mater 2009;167:995.
[19] Zhu C, Wang L, Kong L, Yang X, Wang L, Zheng S, et al. Photocatalytic degradation of azo dyes by supported TiO_2 + UV in aqueous solution. Chemosphere 2000;41:303.
[20] Zainal Z, Hui LK, Hussein MZ, Taufiq-Yap YH, Abdullah AH, Ramli I. Removal of dyes using immobilized titanium dioxide illuminated by fluorescent lamps. J Hazard Mater 2005;B125:113.
[21] Gonçalves MST, Oliveira-Campos AMF, Pinto EMMS, Plasência PMS, Queiroz MJRP. Photochemical treatment of solutions of azo dyes containing TiO_2. Chemosphere 1999;39:781.